Superconductivity in Cu_xTiSe_2

E. MOROSAN[1]*, H. W. ZANDBERGEN[2], B. S. DENNIS[3], J. W. G. BOS[1], Y. ONOSE[4], T. KLIMCZUK[1,5], A. P. RAMIREZ[3], N. P. ONG[4] AND R. J. CAVA[1]*

[1]Department of Chemistry, Princeton University, Princeton, New Jersey 08540, USA
[2]National Centre for HREM, Department of Nanoscience, Delft Institute of Technology, 2628 CJ Delft, The Netherlands
[3]Bell Laboratories, Lucent Technologies, Murray Hill, New Jersey 07974, USA
[4]Department of Physics, Princeton University, Princeton, New Jersey 08540, USA
[5]Faculty of Applied Physics and Mathematics, Gdansk University of Technology, Narutowicza 11/12, 80-952 Gdansk, Poland
*e-mail: emorosan@princeton.edu; rcava@princeton.edu

Published online: 23 July 2006; doi:10.1038/nphys360

Charge density waves (CDWs) are periodic modulations of the density of conduction electrons in solids. They are collective states that arise from intrinsic instabilities often present in low-dimensional electronic systems. The most well-studied examples are the layered dichalcogenides—an example of which is $TiSe_2$, one of the first CDW-bearing materials to be discovered. At low temperatures, a widely held belief is that the CDW competes with another collective electronic state, superconductivity. But despite much exploration, a detailed study of this competition is lacking. Here we report how, on controlled intercalation of $TiSe_2$ with Cu to yield Cu_xTiSe_2, the CDW transition can be continuously suppressed, and a new superconducting state emerges near $x = 0.04$, with a maximum transition temperature T_c of 4.15 K at $x = 0.08$. Cu_xTiSe_2 thus provides the first opportunity to study the CDW to superconductivity transition in detail through an easily controllable chemical parameter, and will provide fundamental insight into the behaviour of correlated electron systems.

Charge density wave (CDW) transitions are a frequent occurrence in transition-metal chalcogenides due to their low structural dimensionality. Layered MX_2 compounds and chain-based MX_3 compounds, where M is a group 4 or 5 metal and X = S, Se or Te, are the best known examples[1–7]. These transitions arise to allow electronic systems to minimize their energy by removing electronic states at the Fermi level. This is achieved by introducing a new structural periodicity at the Fermi wavevector, inducing a bandgap. Superconductivity and the CDW state are two very different cooperative electronic phenomena, and yet both occur because of Fermi surface instabilities and electron–phonon coupling. A number of CDW-bearing materials are also superconducting[8–13], and the idea that superconductivity and CDW states are competing electronic states at low temperatures is one of the fundamental concepts of condensed-matter physics.

The use of control parameters to tune superconducting and CDW transition temperatures has been extensively explored. Pressure (in $NbSe_2$; ref. 14, TaS_3, $(TaSe_4)_2I$ and $NbSe_3$; ref. 10), or doping (in TaS_2; ref. 15), or both (in $Lu_5Ir_4Si_{10}$; ref. 13), have been used to reduce the CDW transition temperature and increase the transition temperature of an existing superconducting state, indicative of the competition between them.

Surprisingly, no system in which the emergence of a superconducting state after a charge-density-wave state has been suppressed through doping has been studied in detail: a transition that implies a deep connection between the two states, that is, that the same electrons are participating in both transitions. $TiSe_2$ was one of the first CDW-bearing compounds known, and is also one of the most frequently studied as the nature of its CDW transition has been controversial for decades. The CDW transition, at approximately 200 K, is to a state with a commensurate $(2a,2a,2c)$ wavevector without an intermediate incommensurate phase[3,16,17]. The commensurate CDW wavevector and electronic structure calculations indicate that, unlike the case in most materials, the CDW in $TiSe_2$ is not driven by Fermi-surface nesting. The normal state is currently believed to be either a semimetal or a semiconductor with a small indirect gap[3,16,18–22]. Recent photoemission experiments[23] concluded that the CDW

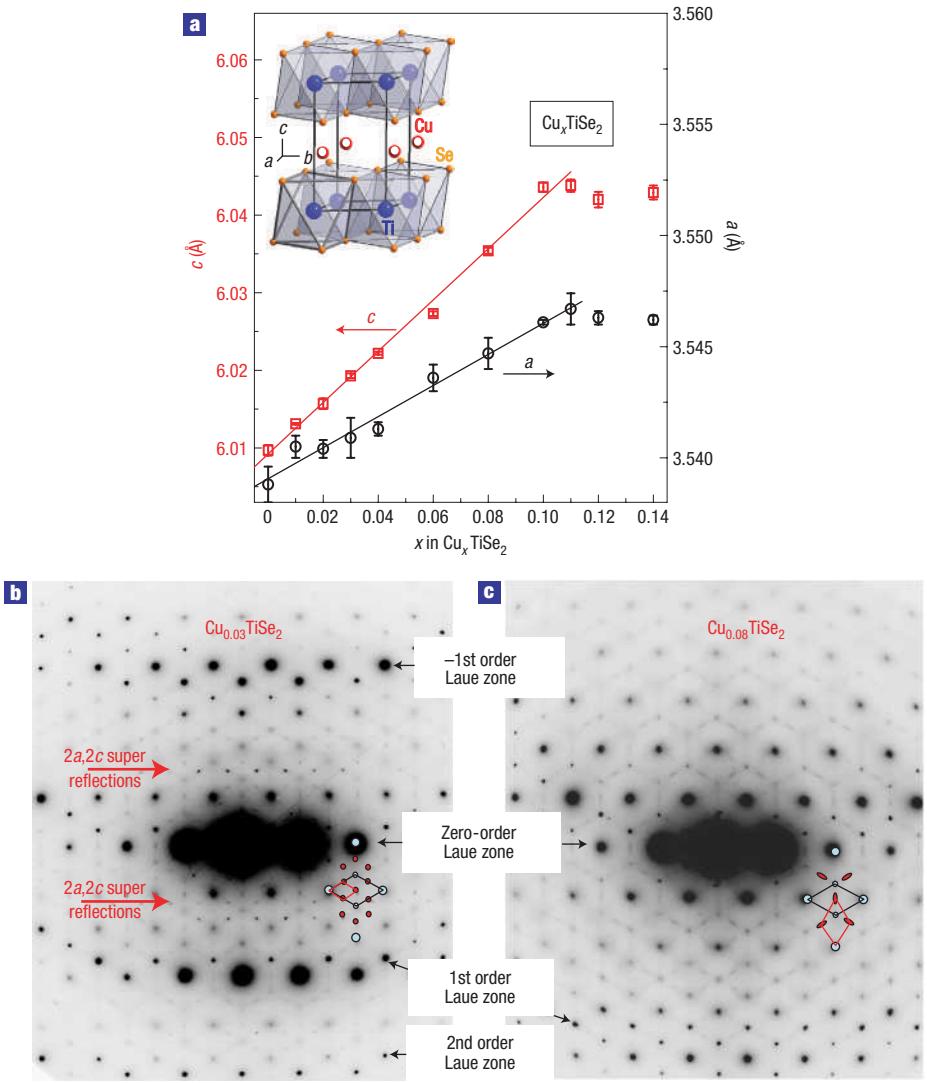

Figure 1 Lattice parameters of Cu_xTiSe_2. **a**, Change in the lattice parameters of Cu_xTiSe_2 with Cu content x, and the respective error bars as generated by the refinement program Bruker AXS Topas. The solid lines reflect the expected Vegards law scaling of a and c with x. Inset: the crystal structure of Cu_xTiSe_2. **b**,**c**, Electron diffraction patterns of the $Cu_{0.03}TiSe_2$ and $Cu_{0.08}TiSe_2$ reciprocal lattices, with the $2a,2c$ supercell outlined. The crystals are tilted away from the (001) zone axis, to show the superreflections in higher-order Laue zones. The diffraction pattern in **b** shows sharp $2a,2c$ superstructure reflections, with the unit cell indicated. The diffraction pattern in **c** shows diffuse superreflections (the unit cell is also shown); these streaked superreflections are also visible in **c**, and are particularly obvious in areas where the $2a,2c$ superstructure is absent.

transition in $TiSe_2$ is a transition from a small indirect gap, semiconductor normal state, into a state with a larger indirect gap at a slightly different location in the Brillouin zone. Although all agree that the CDW transition in $TiSe_2$ is not driven by conventional Fermi-surface nesting, its cause remains controversial, involving a soft phonon and possibly electron–hole coupling or an 'indirect' Jahn–Teller effect[23].

Here we report how, on controlled intercalation of $TiSe_2$ with Cu to yield Cu_xTiSe_2, the CDW transition is continuously suppressed, and a superconducting state emerges near $x = 0.04$ with a maximum T_c of 4.15 K at $x = 0.08$. A CDW–superconductivity phase diagram as a function of doping is developed for Cu_xTiSe_2, analogous to the antiferromagnetism–superconductivity phase diagram found for the high-temperature superconductors. The results indicate that Cu_xTiSe_2 provides the first opportunity to study the CDW–superconductivity transition in detail through an easily controllable chemical parameter. Such studies have been critical in understanding the behaviour of other correlated electron systems, but so far have been lacking in CDW–superconductivity systems.

$TiSe_2$ is a layered compound with trigonal symmetry[24]. The Ti atoms are in octahedral coordination with Se, in $TiSe_2$ layers that, in the pure compound, are bonded to each other by van der Waals forces. As Cu atoms are added, they occupy positions between the $TiSe_2$ layers (Fig. 1a, inset). This results in a systematic expansion of the unit cell with Cu content in Cu_xTiSe_2, as evinced by the lattice parameters shown in Fig. 1a. The expansion of the cell parameters is maintained up to $x = 0.11$. For higher Cu contents, both a and c remain unchanged from their value at $x = 0.11$. It can therefore be concluded that the solubility limit for Cu in $TiSe_2$ is $x = 0.11 \pm 0.01$.

The evolution of the charge density wave with Cu doping is of particular interest. Electron and X-ray diffraction studies of

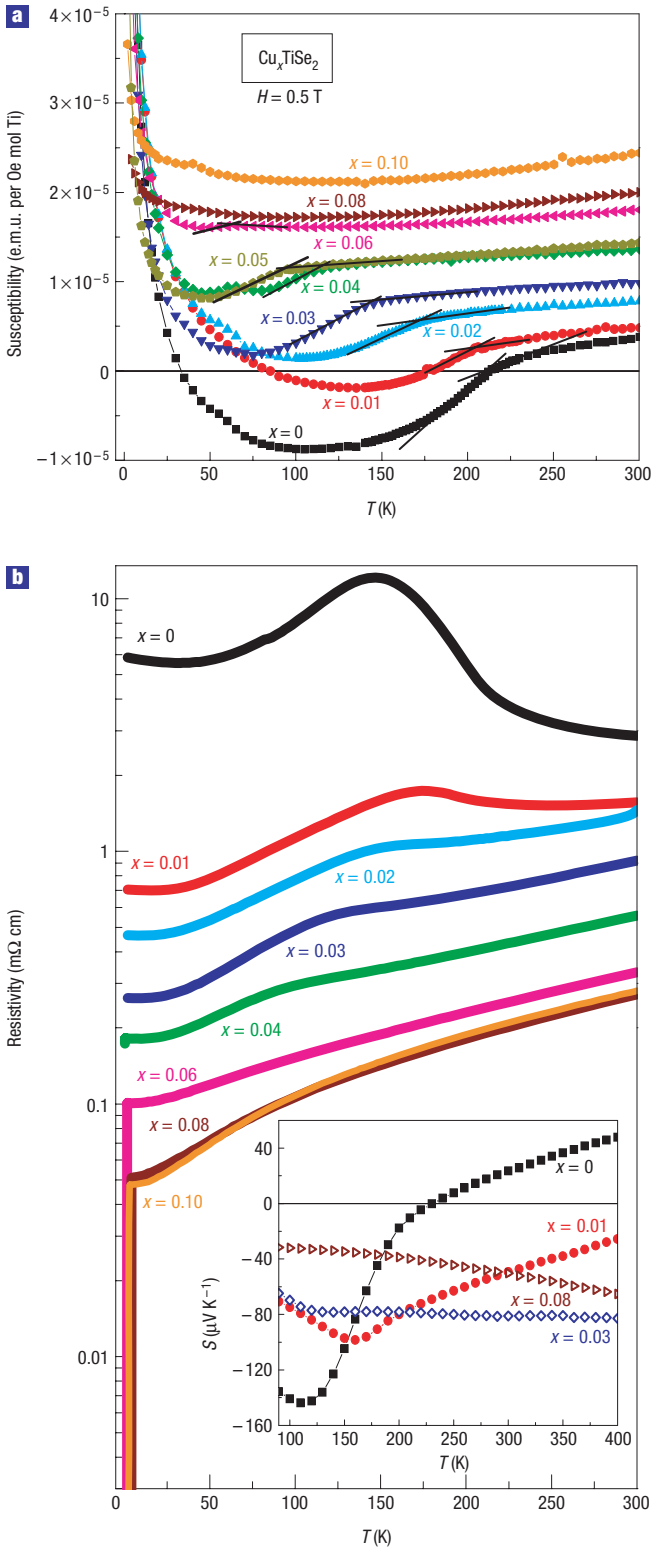

Figure 2 Magnetization and transport properties of Cu_xTiSe_2. a, Cu_xTiSe_2 $M(T)$ curves measured in a constant $H = 0.5$ T applied field, for $0 < x < 0.10$. The solid lines illustrate how the CDW transition temperatures have been determined. (A small peak is seen around 60 K in a few of the measurements, which is attributed to an oxygen impurity trapped in the measurement system.) **b**, $H = 0$ temperature-dependent resistivity data for $0 < x < 0.10$. Inset: Seebeck coefficient for $x = 0$, 0.01, 0.03 and 0.08.

pure $TiSe_2$ at low temperatures show the presence of reflections corresponding to the basic trigonal structure and also the $2a$,$2c$ superstructure reflections associated with the CDW state[3,19]. Figure 1b shows an electron diffraction pattern of $Cu_{0.03}TiSe_2$ taken at approximately 120 K with the crystal tilted away from the [001] zone such that several higher-order Laue zones, with reflections hkl ($l = -1$, 0, 1 and 2) are visible. The superreflections are only observed for $l = 2n + 1$, and are not visible in the zero-order Laue zone in the [001] orientation (where $l = 0$). The $2a$,$2c$ superstructure reflections, as indicated in the figure, are clearly seen, as they are in $TiSe_2$. Therefore, the charge density wave is still present at 120 K at this composition. Significantly, the characteristic CDW wavevector is unchanged by doping. Apart from the $2a$,$2c$ superstructure reflections, which are very sharp and only occur in the higher-order zones where $l = 2n + 1$, more-streaked reflections can be seen. Raising the temperature by approximately 20 K results in the disappearance of the $2a$,$2c$ superstructure reflections. The more-streaked reflections are still present above the CDW transition temperature and remain visible in diffraction patterns taken at room temperature. Furthermore, they are present in the diffraction pattern for $Cu_{0.08}TiSe_2$, the optimal superconducting composition, at 120 K (Fig. 1c) and also in pure $TiSe_2$ at room temperature. The positions of these diffuse peaks are only in part the same as those of the $2a$,$2c$ superstructure, as shown in the overlays. The diffuse superreflections are not confined to a small band at $l = 2n + 1$ but are present everywhere, indicating that they are also streaked along c^* (perpendicular to the $TiSe_2$ planes): the streaking seems to be continuous in that direction. It would be of interest to characterize the diffuse scattering as a function of temperature and composition and determine its origin. It is probably associated with the soft phonon believed to accompany the CDW transition[25].

Figure 2a shows the temperature dependence of the magnetic susceptibilities for Cu_xTiSe_2 over the range of Cu solubility. The normal-state susceptibility (for example, at 300 K) increases with Cu content. This suggests that the Cu doping introduces carriers into the conduction band in $TiSe_2$, increasing the electronic density of states and therefore the Pauli paramagnetism. This is further confirmed by specific heat measurements, described below. A drop in the susceptibility of pure $TiSe_2$ is seen as the temperature is lowered below the CDW transition at 200 K, consistent with the decrease in electronic density of states that occurs on opening a gap at the Fermi level (the susceptibility becomes negative because the core diamagnetism is larger than the Pauli contribution). On doping with increasing amounts of Cu, the CDW state in Cu_xTiSe_2 exists until $x = 0.06$, as seen in the drops in the susceptibilities. The susceptibility drop decreases with increasing Cu content, implying that fewer states are gapped at the CDW transition. The CDW transition temperatures can be determined from the onsets of the susceptibility drops, and decrease continuously with increasing Cu content. For $x = 0.06$, the CDW transition, marked by a very small change in susceptibility, is reduced below 60 K and is no longer visible for higher x. The fact that local moment magnetism is not generated by Cu doping indicates that the intercalated Cu has a formal oxidation state of +1, a $3d^{10}$ electron configuration.

A systematic change in the transport properties of Cu_xTiSe_2 occurs on increasing x. The resistivity of our pure $TiSe_2$ (Fig. 2b) is very similar to that previously reported[3]: a broad maximum occurs around 150 K, with the ratio $\rho(150\,\mathrm{K})/\rho(300\,\mathrm{K}) = 4$, comparable to that of the stoichiometric crystals[3]. However, unlike the single crystals where the ratio $\rho(300\,\mathrm{K})/\rho(6\,\mathrm{K})$ is 3–4, in our sample this ratio is smaller than unity, probably due to the fact that it is a polycrystalline pellet. As shown in Fig. 2b, the resistivity maximum in Cu_xTiSe_2 associated with the CDW state broadens and moves towards lower temperatures with increasing Cu doping,

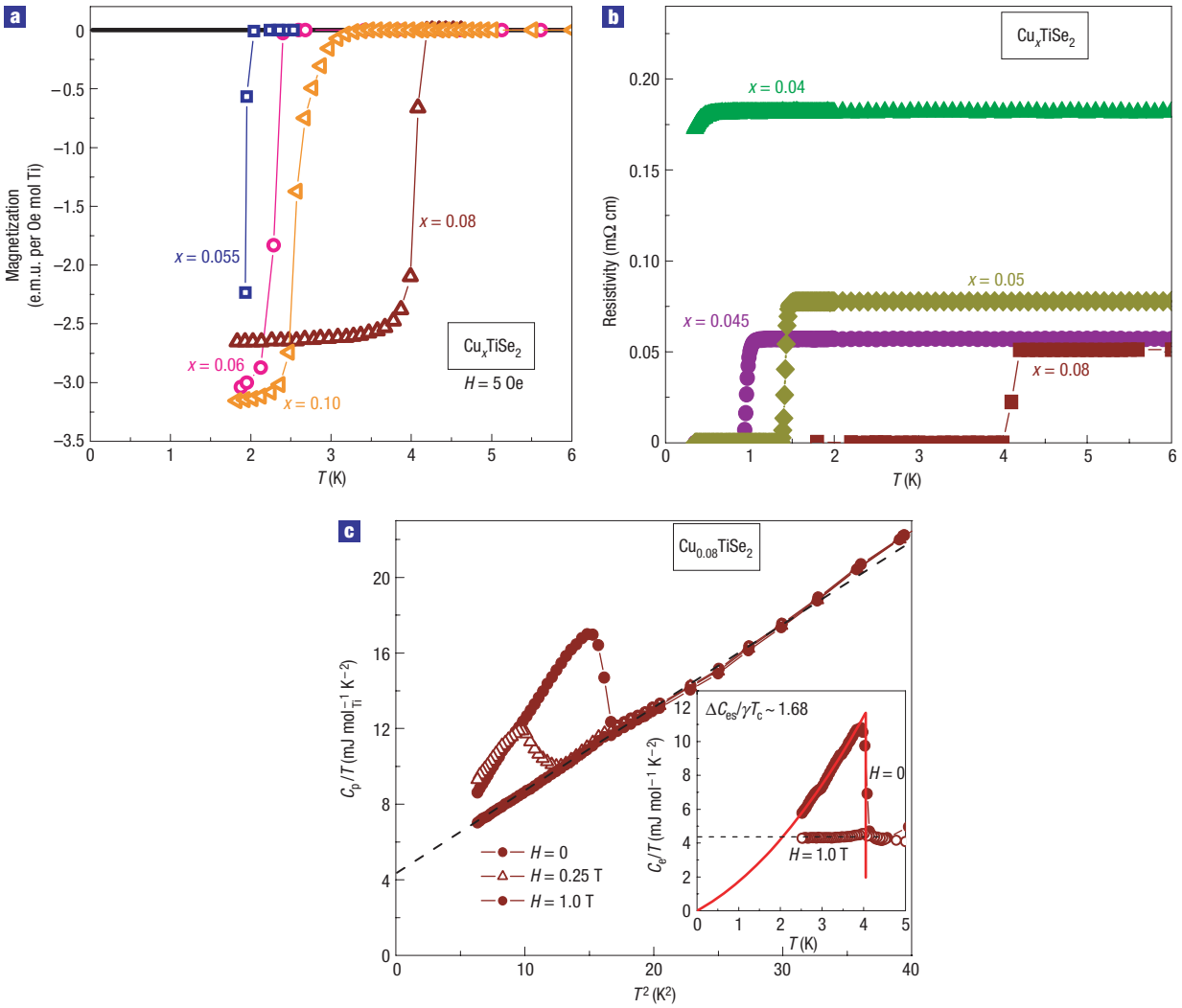

Figure 3 The superconducting phase transition as a function of Cu content *x*. **a**, $H = 5$ Oe a.c. magnetization data at low temperatures, showing the sharp superconducting transitions for $x = 0.055$, 0.06, 0.08 and 0.10. **b**, Low-temperature $\rho(T)$ data in zero field for $x = 0.04$, 0.045, 0.05 and 0.08. **c**, Field-dependent specific heat data around the superconducting transition in $Cu_{0.08}TiSe_2$. The dashed black line represents the extrapolation of the linear fit of $C_p/T(T^2)$ from ~6 K down to 0, yielding an electronic specific heat coefficient γ of 4.3 mJ mol$_{Ti}^{-1}$ K^{-2}. Inset: electronic contribution to the specific heat of the superconducting (filled symbols) and normal (open symbols) state of $Cu_{0.08}TiSe_2$. The solid line represents the entropy-conservation construction, which gives the ratio $\Delta C_{es}/\gamma T_c$ to be ~1.68.

until it becomes unobserved for $x > 0.06$. In addition, the overall resistivities decrease as x increases from 0 to 0.08, and the high-temperature curves become metallic and linear in T. Beyond $x = 0.08$, the normal-state resistivity is almost unchanged. If the ratio $\rho(300\,\mathrm{K})/\rho(6\,\mathrm{K})$ is used to follow the change in transport properties across the series, it can be seen that the smallest amount ($x = 0.01$) of Cu added to $TiSe_2$ yields a fourfold increase in the metallicity. The inset in Fig. 2b illustrates the metal-like behaviour of the Seebeck coefficient (S) in a subset of the Cu_xTiSe_2 compounds. A sharp drop in S for pure $TiSe_2$ around 200 K marks the CDW transition, which is also associated with an apparent change of dominant carrier type (S changes sign). With Cu introduced to this material, the CDW transition is suppressed, and the Seebeck coefficient becomes negative for the whole temperature range shown. For all higher Cu contents, S is negative between 100 and 400 K, and, for example, at the optimal superconducting composition of $x = 0.08$, $|S|$ decreases linearly with T between 400 and 100 K, as expected for a metallic compound. The Seebeck data are thus consistent with electron doping of $TiSe_2$ to a metallic state as Cu is intercalated. Consequently, the susceptibility and transport data indicate that the CDW–metallic transition in Cu_xTiSe_2 is probably due to electron doping away from the ideal value required for CDW formation in $TiSe_2$.

As the Cu_xTiSe_2 compounds evolve into better metals, and the CDW state is suppressed with increasing Cu content, a superconducting state emerges at low temperatures for $x > 0.04$. This is illustrated in the low-temperature magnetization and resistivity data shown in Fig. 3. Below $x = 0.04$, no superconducting transition is observed down to the lowest temperature of our measurements, $T = 0.4$ K. At $x = 0.04$ however, a drop in the resistivity just begins to appear as the temperature is lowered to 0.4 K (Fig. 3b), suggesting the onset of a superconducting transition at that temperature. The superconducting transition is clearly observed for $x = 0.045$ and 0.05 and comes into the temperature range of the susceptibility measurements at $x = 0.055$ (Fig. 3a). T_c reaches a maximum of about 4.15 K for $x = 0.08$ and

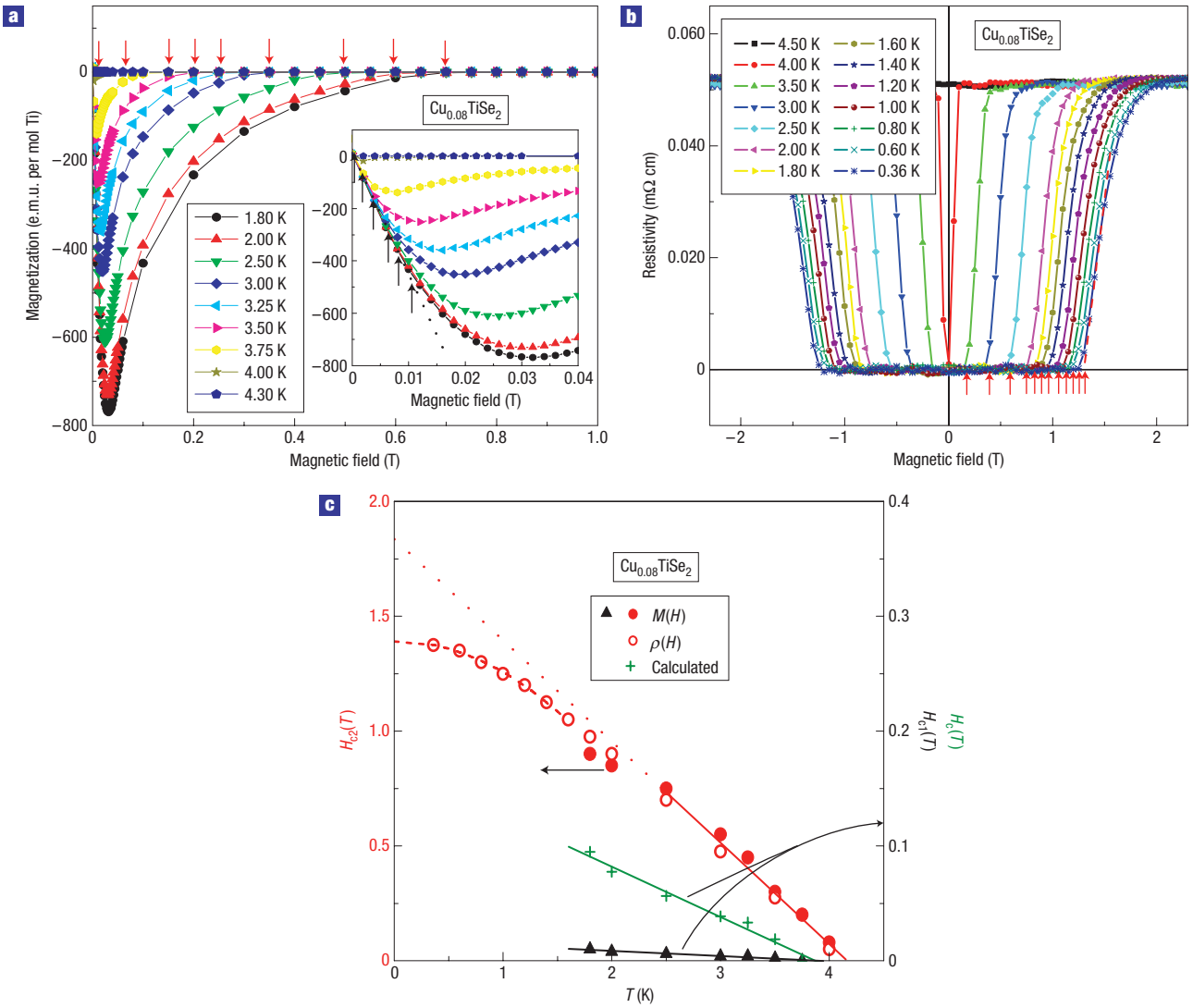

Figure 4 Characterization of the superconductivity in $Cu_{0.08}TiSe_2$. a, $M(H)$ curves for $T = 1.8$, 2.0, 2.5, 3.0, 3.25, 3.5, 3.75, 4.0 and 4.3 K, with red arrows marking the position of $H_{c2}(T)$. Inset: The low-H part, with the position of $H_{c1}(T)$ marked by black arrows. **b**, $\rho(H)$ data for $T = 0.36$, 0.6–2.0 K ($\Delta T = 0.02$ K), and 2.5–4.5 K ($\Delta T = 0.05$ K), with red arrows marking the $H_{c2}(T)$ values. **c**, H_c–T phase diagram, including $H_{c1}(T)$ (triangles) and $H_{c2}(T)$ (circles) determined from $M(H)$ and $\rho(H)$ data, and the calculated thermodynamical critical field $H_c(T)$ calculated as $H_c = \sqrt{(H_{c1} H_{c2})}$ (crosses). As predicted by BCS theory, the solid lines represent linear fits around T_c and the low-temperature dashed line is a fit to $H_{c2}(T) \approx H_{c2}(0)\,[\,1 - 1.07(T/T_c)^2\,]$.

then decreases for higher Cu contents (for example, to 2.5 K for $x = 0.10$). Thus, an optimal composition for superconductivity of $Cu_{0.08}TiSe_2$ is observed.

Specific heat C_p measurements carried out at $H = 0$, 0.25 and 1 T are shown in Fig. 3c as C_p/T versus T^2. As expected, the $H = 0$ specific heat data (filled circles) show a peak at the superconducting transition temperature $T_c = 4.1$ K, which moves down in temperature as magnetic field is applied. The normal-state specific heat can be approximated, at low temperatures, as $C_p = \gamma T + BT^3$, where γT represents the normal-state electron contribution and BT^3 represents the lattice contribution to the specific heat. When plotted as C_p/T versus T^2, the data in Fig. 3c are linear above the transition up to 6 K, and the extrapolation to $T = 0$ gives $\gamma = 4.3\,\mathrm{mJ\,mol^{-1}\,K^{-2}}$. The small γ value and the corresponding superconducting transition temperature $T_c = 4.1$ K place this compound in the T_c versus γ regime of conventional superconductors[26]. The Bardeen–Cooper–Schrieffer (BCS) theory[27] predicts that, at the transition temperature, $\Delta C_e(T_c)/\gamma T_c = 1.49$, and for $Cu_{0.08}TiSe_2$ this ratio, obtained from the entropy conservation construction in the inset in Fig. 3c, is approximately 1.68.

Detailed measurements of the field dependence of the magnetization and the resistive transition of $Cu_{0.08}TiSe_2$, presented in Fig. 4, allow for a better characterization of the superconducting state. The magnetization isotherms for $T = 1.8$–4.3 K (Fig. 4a) exhibit typical type-II superconductor behaviour. Together with the magnetoresistance data (Fig. 4b), these measurements yield the upper critical field values H_{c2} shown as circles in Fig. 4c. The filled circles in Fig. 4c represent the field values where the magnetization becomes 0, and the open circles correspond to the resistance onsets on the $\rho(H)$ curves. Estimates of the lower critical field H_{c1} have been determined from the magnetization data and thus are limited

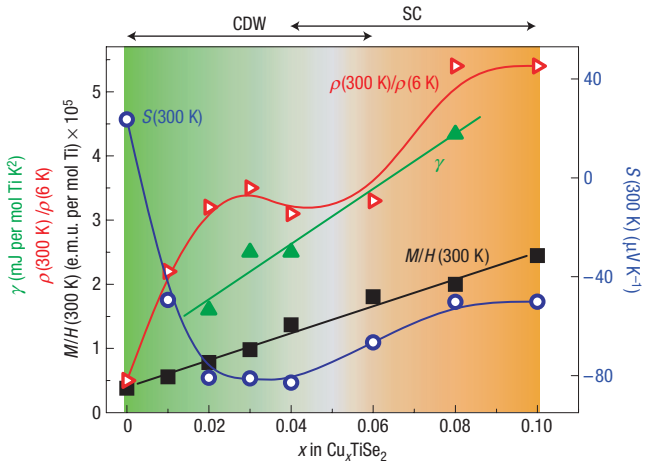

Figure 5 Summary of the composition-dependent properties in Cu_xTiSe_2. M/H (300 K), ρ (300 K)/ρ (6 K), electronic specific heat coefficient γ and Seebeck coefficient S(300 K) as a function of Cu composition x. The solid lines are guides to the eye showing the linear variation of the latter two quantities, whereas for the former two the lines reflect steep changes at low Cu content ($0 < x < 0.02$) and through the superconducting state ($0.04 < x < 0.08$).

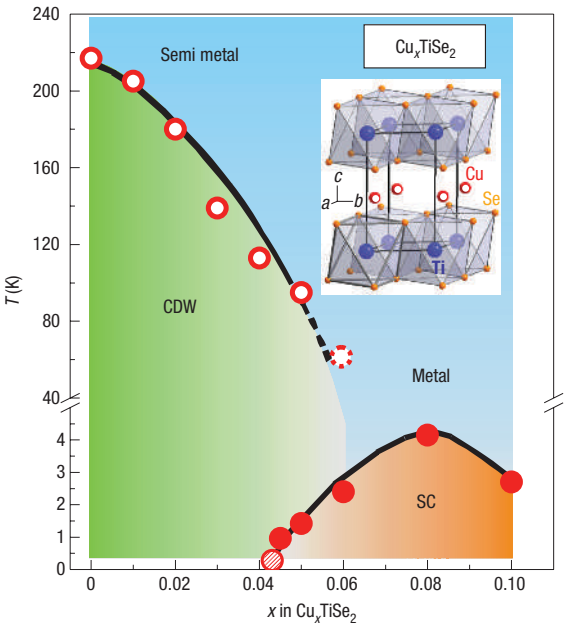

Figure 6 The Cu_xTiSe_2 T–x electronic phase diagram. Open circles represent the CDW transition temperature, and the filled circles correspond to the superconducting transition temperature. The shaded circle at $x = 0.04$ indicates that the transition temperature is just below our minimum available temperature, and the dashed circle at $x = 0.06$ marks the barely visible CDW transition at $x = 0.06$. Inset: Crystal structure of Cu_xTiSe_2.

to temperatures above 1.8 K: as the inset in Fig. 4a shows, the magnetization is linear in field at low H values; H_{c1} is estimated as the field values where departures from linearity occurred at each temperature. The anticipated linear temperature dependence close to T_c is evident for both H_{c1} and H_{c2} (Fig. 4c), which also results in a linear thermodynamic critical field H_c (Fig. 4c), calculated as $H_c = \sqrt{(H_{c1}H_{c2})}$.

Close to $T = 0$, BCS theory predicts that the upper critical field decreases with temperature as $H_c(T) \approx H_c(0)[1 - 1.07(T/T_c)^2]$ (ref. 27). The dashed line in Fig. 4c represents a fit of the H_{c2} data to this expression, yielding a $H_{c2}(0)$ value of approximately 1.39 T. (The zero-field T_c (3.2 K) estimated from this fit is smaller than the measured value of 4.15 K, but the value of $H_{c2}(0)$ is well defined.) The high-temperature data (close to T_c) can also be used to estimate H_{c2}, based on the equation $H_{c2}(0) = 0.693H^*_{c2}(0)$ (ref. 28), where $H^*_{c2}(0) = -(\mathrm{d}H_{c2}/\mathrm{d}T)_{T_c}T_c$. The dotted line in Fig. 4c represents the extrapolation to $T = 0$ of the linear fit at high temperatures, yielding an estimate for $H_{c2}(0) = 1.27$ T. On the basis of these measurements, we conclude that the upper critical field $H_{c2}(0)$ of $Cu_{0.08}TiSe_2$ is $H_{c2}(0) = 1.33 \pm 0.06$ T. Despite exhibiting the expected quadratic temperature dependence at low temperatures, the H_{c2} values determined from field-dependent magnetization, $M(H)$, measurements are probably overestimates of the actual values. This could be a result of using polycrystalline pellets rather than single crystals, particularly if the critical field is anisotropic: the polycrystalline samples yield an average value H_{c2} that is intermediate between the values corresponding to $H \parallel ab$ and $H \parallel c$. Using the above critical field values to estimate the Ginzburg–Landau parameter $\kappa = \lambda/\xi \approx H_{c2}/H_{c1}$ (where λ is the penetration depth, and ξ represents the coherence length), it can be concluded that $Cu_{0.08}TiSe_2$ is in the extreme type-II limit, as $\kappa \approx 1\,\mathrm{T}/0.01\,\mathrm{T} = 100$.

The variation of the transport, magnetic and thermodynamic qualities of the normal state in the Cu_xTiSe_2 series is summarized in Fig. 5. The resistivity, specific heat, magnetic susceptibility and Seebeck coefficient data taken together indicate that the Cu atoms contribute electrons to the conduction band on doping. This electron doping suppresses the CDW and induces metallic behaviour in Cu_xTiSe_2 with a resistivity near $10^{-4}\,\Omega$ cm at room temperature in the metallic phase. As the carriers are introduced, the electronic contribution to the specific heat, γ, increases from approximately 1 to approximately 4 mJ mol^{-1} K^{-2} at the optimal superconducting composition. Estimates of the Wilson ratio $R = \chi_0/(3\gamma)(\pi k_B/\mu_B)^2$ (where χ_0 is the temperature-independent susceptibility, k_B is the Boltzmann's constant and μ_B is the Bohr magneton) based on the measured susceptibilities alone yield values between 0.3 and 0.4, much smaller than the expected $R = 1$ value for the free-electron approximation. The small susceptibilities observed in this system must be corrected for core diamagnetism; however, correcting for the core contributions of Ti^{4+} and Se^{2-} (ref. 29) results in R values that seem to be too high (between 2.5 and 5). This suggests that additional contributions to the observed susceptibility need to be considered to fully understand this system. This analysis is left to a future study.

Finally, the overall behaviour of this system is summarized in the electronic phase diagram presented in Fig. 6. Using Cu doping as a finely controlled tuning parameter, the CDW transition in $TiSe_2$ is driven down in temperature, and a new superconducting state emerges. The superconducting state appears for $x > 0.04$, going through a maximum T_c of 4.15 K at $x = 0.08$, followed by a decrease of T_c before the chemical phase boundary is reached at $x = 0.11$. There is a small boundary composition region ($0.04 < x < 0.06$) where superconductivity and CDW behaviour seem to coexist. The reason why superconductivity arises from the CDW state in $TiSe_2$ on Cu doping has not yet been determined. It may be that Cu doping results in a tendency towards increasing the dimensionality of the Fermi surface, destabilizing the CDW and allowing for correlations to build in a third dimension, tipping the balance in favour of superconductivity. Otherwise, superconductivity may emerge from the CDW state due to the change in electron count on Cu doping. Further study of Cu_xTiSe_2 will determine which of these

is the underlying cause of the transition between the competing CDW and superconducting states, as will additional detailed and generic studies made possible by the fine chemical tuning of the electronic system that Cu_xTiSe_2 affords.

METHODS

Polycrystalline Cu_xTiSe_2 samples ($0 \leq x \leq 0.14$) were prepared in two steps. First, stoichiometric amounts of elemental powders were sealed in evacuated silica tubes and heated from room temperature to 350 °C in about 1 h. The temperature was then increased at 50 °C h^{-1} to 650 °C, after which it was maintained at 650 °C for 20 h. Second, the powders were pressed into pellets, resealed in silica tubes under vacuum, and annealed at 650 °C for 50 h. Homogeneous, purple–grey pellets were obtained.

Powder X-ray diffraction measurements were used to characterize the samples. Room-temperature data were recorded on a Bruker D8 diffractometer, using Cu Kα radiation and a diffracted beam monochromator. Electron diffraction was carried out with Philips CM300UT and CM30T electron microscopes, operated at 300 kV, using image plates as recording media. Electron transparent areas of the specimens were obtained by crushing slightly under ethanol to form a suspension, and then placing a droplet of this suspension on a carbon-coated holey film on a Cu or Au grid. For the cooling experiments, a Gatan liquid nitrogen cooling holder was used for the CM30T, and a home-made one was used for the CM300UT. The Gatan holder allows for an estimation of the sample temperature, but it is measured far from the sample area, resulting in an underestimate of the sample temperature. Low-temperature diffraction data were taken primarily at an indicated temperature of 87 K, but, because the temperature is measured away from the sample cap (as described above), we estimate the lowest temperature reached to be approximately 100–120 K. The heating of the sample due to the electron beam could also be a factor, but we excluded this as the major effect by measurements with low beam intensities.

Magnetization measurements as a function of temperature and applied field were carried out in a Quantum Design MPMS superconducting quantum interference device magnetometer. Temperature-dependent resistivity measurements in constant applied fields were taken in a Quantum Design PPMS-9 instrument, using a standard four-probe technique. Additional resistivity measurements down to $T = 0.4$ K were carried out in a ^{3}He refrigerator inserted in a 7 T superconducting magnet. Thermopower data were collected using an MMR technologies SB100 Seebeck measurement system. Specific heat data were also collected in the Quantum Design PPMS-9 instrument, by the thermal relaxation method.

Received 6 May 2006; accepted 28 June 2006; published 23 July 2006.

References

1. Wilson, J. A. & Yoffe, A. D. The transition metal dichalcogenides discussion and interpretation of the observed optical, electrical and structural properties. *Adv. Phys.* **28,** 193–335 (1969).
2. Wilson, J. A., Di Salvo, F. J. & Mahajan, S. Charge-density waves and superlattices in the metallic layered transition metal diehaleogenides. *Adv. Phys.* **24,** 117–201 (1975).
3. Di Salvo, F. J., Moncton, D. E. & Waszczak, J. V. Electronic properties and superlattice formation in the semimetal $TiSe_2$. *Phys. Rev. B* **14,** 4321–4328 (1976).
4. Kim, S. J. *et al.* AFM image visualization of layered dichalcogenides, 1T-MTe(2) (M = V, Ta). *J. Phys. Chem. Solids* **58,** 659–663 (1997).
5. Kasuya, T., Jung, M. H. & Takabatake, T. Charge density wave and excitonic magnetic polarons in $CeTe_2$. *J. Magn. Magn. Mater.* **220,** 235–258 (2000).
6. Boswell, F. W. & Bennett, J. C. Density waves in Nb_3Te_4: Effects of indium and thallium intercalation. *Mater. Res. Bull.* **31,** 1083–1092 (1996).
7. Wang, C., Slough, C. G. & Coleman, R. V. Spectroscopy of dichalcogenides and trichalcogenides using scanning tunneling microscopy. *J. Vac. Sci. Technol. B* **9,** 1048–1051 (1991).
8. Nagata, S. *et al.* Superconductivity in the layered compound 2H-TaS_2. *J. Phys. Chem. Solids* **53,** 1259–1263 (1992).
9. Kumakura, T., Tan, H., Handa, T., Morishita, M. & Fukuyama, H. Charge density wave and superconductivity in 2H-$TaSe_2$. *Czech. J. Phys.* **46,** 2611–2612 (1996).
10. Nunezregueiro, M., Mignot, J. M., Jaime, M., Castello, D. & Monceau, P. Superconductivity under pressure in linear chalcogenides. *Synth. Met.* **56,** 2653–2659 (1993).
11. Mihaila, B. *et al.* Pinning Frequencies of the collective modes in α-uranium. *Phys. Rev. Lett.* **96,** 76401 (2006).
12. Jaiswal, D. *et al.* Superconducting parameters of a CDW compound $Lu_5Ir_4Si_{10}$. *Physica B* **312,** 142–144 (2002).
13. Singh, Y., Nirmala, R., Ramakrishnan, S. & Malik, S. K. Competition between superconductivity and charge-density-wave ordering in the $Lu_5Ir_4(Si_{1-x}Ge_x)_{10}$ alloy system. *Phys. Rev. B* **72,** 45106 (2005).
14. Morris, R. C. Connection between charge-density waves and superconductivity in $NbSe_2$. *Phys. Rev. Lett.* **34,** 1164–1166 (1975).
15. Fang, L. *et al.* Fabrication and superconductivity of Na_xTaS_2 crystals. *Phys. Rev. B* **72,** 14534 (2005).
16. Bachrach, R. Z. & Skibowski, M. Angle-resolved photoemission from $TiSe_2$ using synchrotron radiation. *Phys. Rev. Lett.* **37,** 40–42 (1976).
17. Woo, K. C. *et al.* Superlattice formation in titanium diselenide. *Phys. Rev. B* **14,** 3242–3247 (1976).
18. Wilson, J. A. Concerning the semimetallic characters of TiS_2 and $TiSe_2$. *Solid State Commun.* **22,** 551–553 (1977).
19. Zunger, A. & Freeman, A. J. Band structure and lattice instability of $TiSe_2$. *Phys. Rev. B* **17,** 1839–1842 (1978).
20. Myron, H. W. & Freeman, A. J. Electronic structure and optical properties of layered dichalcogenides: TiS_2 and $TiSe_2$. *Phys. Rev. B* **9,** 481–486 (1974).
21. Isomaki, H., Boehm, J. von & Krusius, P. Band structure of group IVA transition-metal dichalcogenides. *J. Phys. C* **12,** 3239–3252 (1979).
22. Stoffel, N. G., Kevan, S. D. & Smith, N. V. Experimental band structure of 1T-$TiSe_2$ in the normal and charge-density-wave phases. *Phys. Rev. B* **31,** 8049–8055 (1985).
23. Kidd, T. E., Miller, T., Chou, M. Y. & Chiang, T.-C. Electron-hole coupling and the charge density wave transition in $TiSe_2$. *Phys. Rev. Lett.* **88,** 226402 (2002).
24. Oftedal, I. Roentgenographische Untersuchungen von SnS_2, $TiS2_2$, $TiSe_2$, $TiTe_2$. *Z. Phys. Chem.* **134,** 301–310 (1928).
25. Bussmann-Holder, A. & Buttner, H. Charge-density-wave formation in $TiSe_2$ driven by an incipient antiferroelectric instability. *J. Phys. Condens. Matter* **14,** 7973–7979 (2002).
26. Batlogg, B *et al.* Superconductivity in Bi-O and Sb-O perovskites. *Physica C* **162–164,** 1393–1396 (1989).
27. Bardeen, J., Cooper, L. N. & Schrieffer, J. R. Theory of superconductivity. *Phys. Rev.* **108,** 1175–1204 (1957).
28. Hake, R. R. Upper-critical-field limits for bulk type-II superconductors. *Appl. Phys. Lett.* **10,** 189–192 (1967).
29. Carlin, R. L. *Magnetochemistry* (Springer, New York, 1986).

Acknowledgements

This research was supported primarily by the US DOE-BES solid state chemistry program, and, in part, by the US NSF MRSEC program.
Correspondence and requests for materials should be addressed to E.M. or R.J.C.

Competing financial interests

The authors declare that they have no competing financial interests.